A Shock-Absorbing Non-Hydrostatic Solver on σ-Grids for Wave Modeling Over Complex Bathymetry

Hans Bihs, Ronja Ehlers and Widar Wang *

Abstract

Due to the high computational cost of computational fluid dynamics (CFD), various faster numerical wave tanks (NWT) have been developed for large-scale wave propagation, such as high-order spectral (HOS) models and fully nonlinear potential flow (FNPF) models. These models often neglect turbulence and viscosity, which are important for coastal processes such as wave-current interactions and sediment transport. Thus, a fast wave model that can incorporate turbulence and viscosity is in demand. This research presents a three-dimensional non-hydrostatic model called REEF3D::NHFLOW, which operates on a moving σ-grid. By solving the non-hydrostatic Navier-Stokes equations, this model provides detailed results. The grid used in REEF3D::NHFLOW follows the surface and bottom topography, allowing for grid refinement near the water surface or bottom while maintaining low computational effort. Developed within the open-source hydrodynamics framework REEF3D, the new model is fully parallelized and utilizes the domain decomposition strategy and MPI communication between processors. This paper showcases the capabilities of this new and efficient one-phase flow model through the implementation of a free surface and bottom following σ-grid approach. The benchmark validations on steep 5^{th}-order Stokes waves, wave decomposition over a submerged bar, focused waves and wave breaking over a mild slope demonstrate the model's accuracy and stability for both deep water dispersive waves and coastal nonlinear waves transformations. The engineering relevance of the model is demonstrated through full-scale simulations of wave propagation into the Naissaar harbour and breaking wave formations over submarine canyons at Nazaré.

Keywords: Artificial Intelligence, Machine learning, Neural Network, Numerical wave modeling, Coastal marine structures, Down-scale analysis

1 Introduction

A range of computational fluid dynamics (CFD) based numerical wave tanks (NWT) have been introduced that resolve the wave propagation and the associated wave hydrodynamics in

*Corresponding author, widar.w.wang@ntnu.no
Postprint, published in JOMAE, doi:http://dx.doi.org//10.1115/1.4068917

great detail. Popular examples are the OpenFOAM based NWTs waves2Foam Jacobsen et al. (2012) or OlaFLow Higuera et al. (2013), where a two-phase flow approach and the VOF-method for the free surface are used. A level set method based NWT was presented as part of the REEF3D open-source hydrodynamics framework Bihs et al. (2016) with a focus on breaking waves Kamath et al. (2017), breaking wave forces on cylindrical Aggarwal et al. (2019a), porous Sasikumar et al. (2020) and jacket structures Aggarwal et al. (2019b). For a variety of ocean and coastal engineering scenarios, a faster solution of nonlinear wave propagation is desirable. High-order spectral (HOS) (see e.g. Ducrozet et al. (2012)) wave models and fully nonlinear potential flow (FNPF) models (e.g. Engsig-Karup et al. (2009), Grilli et al. (1994) or Wang et al. (2022c)) are possible candidates for fast wave propagation simulations in deep water. For example, designing offshore wind substructures often requires the identification of significant wave events, currents and sediment transport processes combined. The dynamics of each phenomenon are strongly correlated and contribute to the investigated situation such as their impact on the offshore structures. A potential flow model is capable to represent large-scale wave propagations. However, for wave-current interaction, sediment transport or swash zone dynamics, viscous flow models that can include the effects of turbulence are more suitable. Casulli and Stelling Casulli and Zanolli (2002) presented a fractional step solution to the three-dimensional Navier-Stokes equations on unstructured grids including a solution for the dynamic component of the pressure. The model was validated for wave propagation over a submerged bar. Compared to more recent approaches, a relatively large amount of vertical cells was needed (32 vertical elements) to capture the highly dispersive waves after decomposition. After presenting a highly innovative fully nonlinear potential flow solver on a σ-coordinate grid Li and Fleming (1997), Li and Fleming Li and Fleming (2001) showed the solution for the 3D Navier-Stokes equations on a similar grid architecture. They could reproduce relatively accurate results for wave propagation over a submerged bar with a reasonable number of vertical grid points (11 vertical elements). Later, Li Li (2008) presented a modified version of this model with a cut cell approach for the cells at the free surface. Another σ-coordinate grid solver was presented with a fully collocated variable arrangement Lin and Li (2002). It uses extrapolation to enforce the zero non-hydrostatic pressure condition at the free surface, requiring relatively large number of vertical cells for capturing dispersive waves.

More recent successful and well-known implementations of three-dimensional Navier-Stokes solvers using a σ-coordinate grid are the open-source solvers SWASH Stelling and Zijlema (2003)Zijlema et al. (2005) and NHWAVE Ma et al. (2012)Ma et al. (2013). The σ-coordinate allows for precise locations of the boundary conditions as it normalises the vertical coordinates between 0 and 1 and intuitively adapts to the varying bathymetries. Free-surface refinements in a σ coordinate also improve accuracy with fewer cells. However, the vertical grid refinement may require calibrations as indicated in Pákozdi et al. (2021). SWASH pursues a staggered grid configuration for the velocities and a Keller-box scheme Stelling and Zijlema (2003) for the non-hydrostatic pressure in order to enforce the zero-pressure at the free surface directly. With a correction approach for the pressure and a semi-implicit finite volume approximation for the velocity and free surface equations, SWASH is able to deliver impressive dispersion characteristics. Wave problems with high nondimensional water depth kd numbers can be solved accurately with relatively few vertical grid layers, where k is the wave number and d is the still water depth. NHWAVE takes a different approach, employing a Godunov-type scheme with velocities located at the cell centers Ma et al. (2012). Similar to SWASH, the pressure is defined at the horizontal grid lines in order to prescribe an accurate free surface

boundary condition.

The current paper presents the new three-dimensional non-hydrostatic model NHFLOW, implemented into the open-source hydrodynamics framework REEF3D (see e.g. Wang et al. (2020*b*)Wang et al. (2020*a*)) deployed on a σ-coordinate grid. The framework aims at representing phase-resolved waves and hydrodynamics at all relevant scales, from large-scale deep to shallow water wave propagation at the Norwegian coast Wang et al. (2023), over coastal wave modeling Reidulff et al. (2023) to high-resolution modeling of near-shore breaking wave kinematics Aggarwal et al. (2020). Several multi-physics extensions relevant to the field of offshore engineering have been integrated, e.g. for modeling of local scour around offshore wind turbines Ahmad et al. (2020) or complex fluid-structure interaction Wang et al. (2022*a*), including a mooring model Martin et al. (2021) and a dynamic net algorithm Martin and Bihs (2021). The new model is aimed to be complementary to the other models within the REEF3D framework and combine their strengths as well. It is purposed for more computationally efficient than the CFD model REEF3D::CFD Bihs et al. (2016). It is designed to incorporate viscosity and turbulence, in contrast to the fully nonlinear potential flow model REEF3D::FNPF Bihs et al. (2020); Wang et al. (2022*c*, 2023), and it is expected to be less restricted by the water depth than the nonhydrostatic shallow water model REEF3D:: SFLOW Wang et al. (2020*b*). The models specialise on different applications and can be used together through the hydrodynamic coupling approach Wang et al. (2022*b*); Dempwolff et al. (2023).

Similar to NHWAVE, REEF3D::NHFLOW uses a Godunov-type scheme for shock-capturing properties, albeit with WENO flux reconstruction. In order to achieve good dispersion characteristics, a pressure correction method is used, similar to SWASH. As part of the REEF3D framework, MPI parallelization, hypre's geometrid multigrid solvers Ashby and Falgout (1996), and high-order finite difference discretization methods are readily available.

The highlights of the new model can be summarised as follows: 1) Fifth-order WENO (weighted essentially non-oscillatory) flux reconstruction for the HLL (Harten–Lax–van Leer) Riemann solver for improved accuracy and stability. 2) The non-hydrostatic pressure correction scheme for improved vertical flow structure and wave dispersion. 3) The deferred correction approach Peric and Ferziger (2001) that reduces the complexity of the matrix resulting from the Poisson equation, and thus improves the computational efficiency.

In the coastal areas, the wave transformations are very nonlinear and wave interactions with complex coastal structures show challenging hydrodynamic behaviours, as have been amply shown before Keerthi Raaj et al. (2023); Praveen et al. (2022); Kumaran et al. (2024). In the following, NHFLOW is validated against different scenarios for dispersive waves and nonlinear coastal wave transformations over varying bathymetry. The possibilities of the new model for large-scale engineering applications are demonstrated with two real-world cases.

2 Numerical Model

The model REEF3D::NHFLOW solves the continuity, free surface and the three-dimensional Euler equations in the following format:

$$\begin{aligned} &\frac{\partial u_i}{\partial x_i} = 0 \\ &\frac{\partial hu_i}{\partial t} + u_j \frac{\partial hu_i}{\partial x_j} = -\frac{h}{\rho}\frac{\partial p}{\partial x_i} - hg_i \end{aligned} \tag{1}$$

In the current paper, the focus is on pure wave propagation problems, thus the influence of the viscosity is neglected. Extending the code to capture viscous flow is straightforward by including the viscous stresses in Eq. 1. The following equation solves the dynamic free surface equation:

$$\frac{\partial h}{\partial t} + \frac{\partial h u_i}{\partial x_i} = 0 \tag{2}$$

The one-phase flow model selects the efficient approach of a free surface and bottom following σ-grid Li and Fleming (1997). The z-coordinate in the vertical direction is then transformed using the definition of the water depth $h(x, y, t) = \eta(x, y, t) + d(x, y)$. The parameter d gives the distance from the bed to the still water level.

$$\sigma = \frac{z + h(x, y, t)}{d(x, y)} \tag{3}$$

The σ-coordinate system is both bathymetry and free surface following, thus the terms for the σ-coordinate transformation can be calculated as follows Madsen (2009):

$$\begin{aligned}
\frac{\partial \sigma}{\partial t} &= \frac{\sigma}{h}\frac{\partial h}{\partial t} \\
\frac{\partial \sigma}{\partial x} &= (1-\sigma)\,\frac{1}{h}\frac{\partial d}{\partial x} - \sigma\frac{1}{h}\frac{\partial \eta}{\partial x} \\
\frac{\partial \sigma}{\partial y} &= (1-\sigma)\,\frac{1}{h}\frac{\partial d}{\partial y} - \sigma\frac{1}{h}\frac{\partial \eta}{\partial y} \\
\frac{\partial \sigma}{\partial z} &= \frac{1}{h}
\end{aligned} \tag{4}$$

The governing equations can be written in vector form:

$$\frac{\partial \mathbf{U}}{\partial t} + \frac{\partial \mathbf{F}(\mathbf{U})}{\partial x} + \frac{\partial \mathbf{G}(\mathbf{U})}{\partial y} + \frac{\partial \mathbf{H}(\mathbf{U})}{\partial \sigma} = \mathbf{S} \tag{5}$$

Following the concept of the conservative shallow water equations (see e.g. Roeber et al. (2010) or Ma et al. (2012)), the individual vector components can be written as follows:

$$\mathbf{F} = \begin{bmatrix} hu \\ hu^2 + \frac{1}{2}g\eta^2 + g\eta d \\ huv \\ huw \end{bmatrix} \quad \mathbf{G} = \begin{bmatrix} hv \\ huv \\ hu^2 + \frac{1}{2}g\eta^2 + g\eta d \\ huw \end{bmatrix} \quad \mathbf{H} = \begin{bmatrix} \omega \\ u\omega \\ v\omega \\ w\omega \end{bmatrix} \tag{6}$$

The source term vectors contain the bed gradient term from the hydrostatic pressure gradient splitting Liang and Marche (2009) as well as the non-hydrostatic pressure gradient.

$$\mathbf{S} = \begin{bmatrix} 0 \\ g\eta\frac{\partial d}{\partial x} - \frac{h}{\rho}\left(\frac{\partial p}{\partial x} + \frac{\partial p}{\partial \sigma}\frac{\partial \sigma}{\partial x}\right) \\ g\eta\frac{\partial d}{\partial y} - \frac{h}{\rho}\left(\frac{\partial p}{\partial y} + \frac{\partial p}{\partial \sigma}\frac{\partial \sigma}{\partial y}\right) \\ -\frac{h}{\rho}\frac{\partial p}{\partial z}\frac{\partial \sigma}{\partial z} \end{bmatrix} \tag{7}$$

The relative vertical velocity ω in the σ-coordinate frame replaces the vertical velocity w in the governing equations. This way, the σ-transformation terms are included in the convection discretization without the need to add them explicitly. The relative vertical velocity ω is defined as:

$$\omega = h\left(\frac{\partial \sigma}{\partial t} + u\frac{\partial \sigma}{\partial x} + v\frac{\partial \sigma}{\partial y} + w\frac{\partial \sigma}{\partial z}\right) \tag{8}$$

The velocities and the free surface are advanced in time with a second-order TVD (total variation diminishing) Runge-Kutta scheme Gottlieb and Shu (1998) together with adaptive time stepping based on the CFL (Courant–Friedrichs–Lewy) criterion. A Godunov-type scheme is employed to solve for the conserved variables h, hu, hv and hw, which are located at the cell centers. The cell face fluxes are approximated with an HLL (Harten–Lax–van Leer) Riemann Harten et al. (1983) solver with the left and right fluxes reconstructed using the 5th-order WENO (weighted essentially non-oscillatory) scheme Jiang and Shu (1996). A projection method for the non-hydrostatic pressure correction Chorin (1968) is solved. The resulting Poisson equation is solved with hypre's conjugated gradient solver BiCGTAB (biconjugate gradient stabilized) van der Vorst (1992) together with geometric multigrid preconditioner PFMG Ashby and Falgout (1996).

The model is fully parallelized using the domain decomposition approach and MPI (message passing interface) Forum (1994). Waves can be generated Jacobsen et al. (2012) and absorbed Chen et al. (2019) with relaxation zones or alternatively with actively absorbing Dirichlet inlets and outlets Higuera et al. (2013). A wetting and drying algorithm captures the dynamically moving wet-dry interface, see e.g. Roeber et al. (2010)Roeber and Cheung (2012) for more information. Due to its shock-capturing characteristics, the model runs stably without the need for a dedicated breaking wave model.

3 Validation

3.1 5th-order Stokes Waves

At first, the new numerical model is tested in an empty two-dimensional wave tank with a total length of $L = 200$ m and a still water depth of $d = 4.01$ m. Based on the wave conditions tested in Pakozdi et al. Pakozdi et al. (2021), Fenton's 5th-order Stokes wave theory Fenton (1985)Kinnas (2007) with a wave height of $H = 1.0$ m, wave period $T = 4.5$ s and a resulting wave length $L = 25.03$ m is used to generate waves using the relaxation method. One wavelength is chosen to relax the wave generation zone and two wavelengths are selected for the numerical beach relaxation. For the numerical model REEF3D::NHFLOW, 5 vertical layers with a moderated vertical numerical stretching (exponential stretching towards the free surface with factor 2.5) are found to be sufficient to accurately predict magnitude and phase of the propagating nonlinear waves. Fig. 1 shows the sensitivity study regarding the horizontal grid resolution. For 100 horizontal cells, a pronounced phase shift and some wave attenuation can be observed. Increasing the horizontal cell count to 175 keeps the wave height intact, but still leaves a visible phase shift. At 250 cells, the agreement between REEF3D::NHFLOW and the 5th-order Stokes theory is already very good. From 350 cells onward, the numerical model has converged to the theoretical free surface elevation exactly. This means that, for the given wave conditions, 44 cells per wavelengths are sufficient. A CFL number of 1.0 is used and all simulations are run to $T = 120$ s.

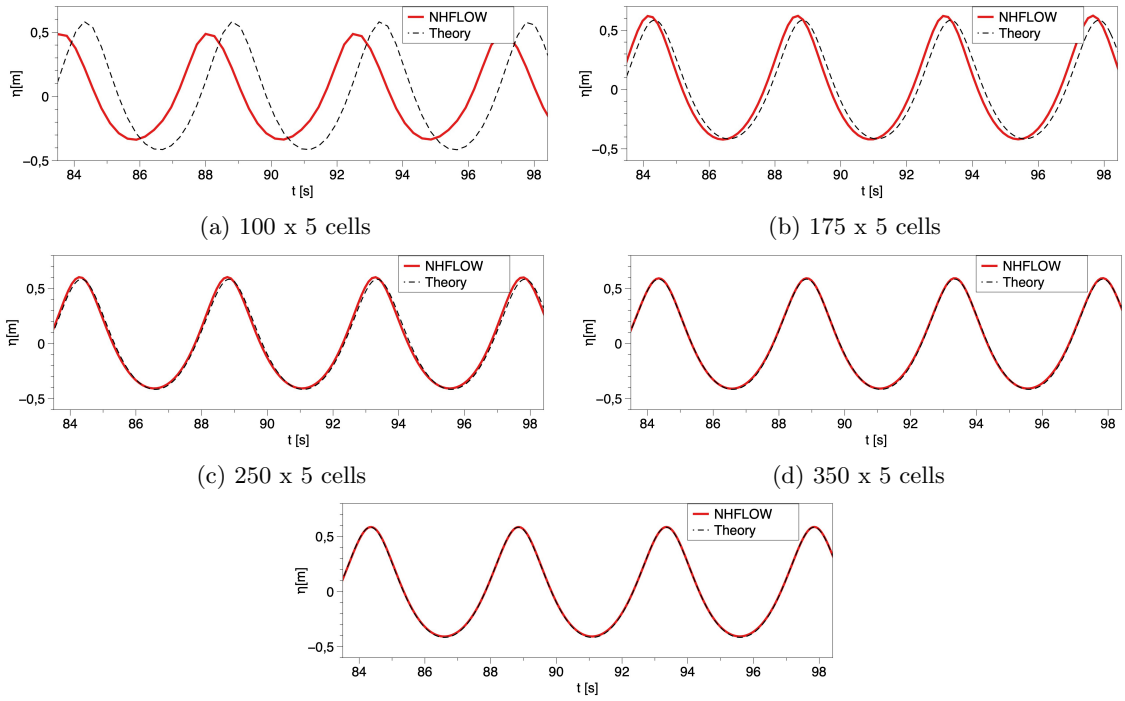

(a) 100 x 5 cells

(b) 175 x 5 cells

(c) 250 x 5 cells

(d) 350 x 5 cells

(e) 500 x 5 cells

Figure 1: Surface elevations for 5th-order Stokes waves with $H = 1$ m, $T = 4.5$ m and $d = 4.01$ m using REEF3D::NHFLOW in a 200 m long wave tank. The wave gage is located at $x = 125$ m.

3.2 Submerged Bar

The new non-hydrostatic wave model is validated against the experiment by Beji and Battjes (1993). Here, 2nd-order Stokes waves with a wave height $H = 0.021$ m and a wave period of $T = 2.525$ s are generated. The waves propagate towards the front slope of the submerged bar with a slope of 1:20, where the waves shoal but do not break. On top of the bar and on the 1:10 downward-directed slope, the waves are decomposed into their higher-order harmonics. This setup and hydrodynamic behaviour make the submerged bar experiment a highly relevant test case for testing the dispersion capabilities of the wave model, as relatively short waves with large kd values are generated. The experimental setup and the locations of the 8 wave gages are shown in Fig. 2.

The numerical model uses 1400 cells in x-direction and 3 vertical layers with exponential stretching toward the free surface (exponential stretching factor 2.5). The horizontal grid resolution convergence study shown in Fig.3 results in a constant $dx = 0.027$ m. A CFL number of 1.0 is used to determine the time step size. The simulation is run for $T = 60$ s. After the waves have passed the submerged bar, higher-order harmonics are formed that result in highly dispersive waves. Overall, the model maintains the wave amplitudes and phase well throughout the wave tank compared to the measurements. The results demonstrate the capability to simulate complex wave transformation over a varying bed topography with a relatively coarse mesh.

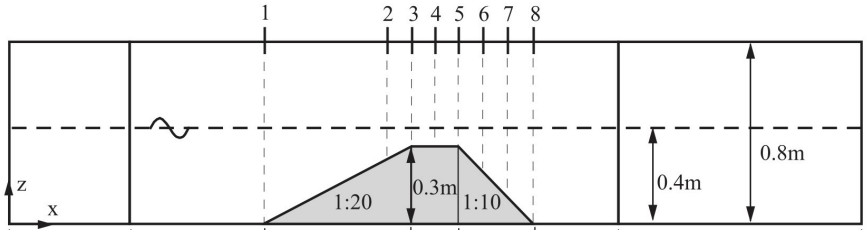

Figure 2: Wave gage placement for the submerged bar test case.

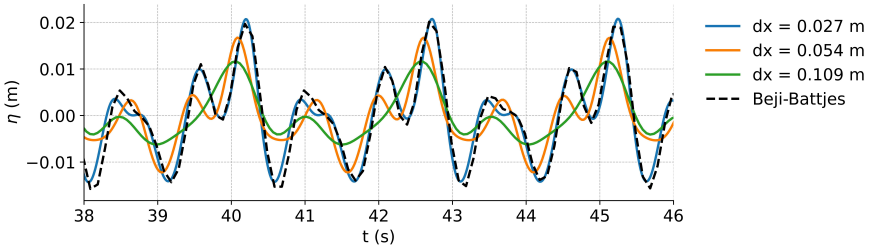

Figure 3: grid convergence at gage 8

3.3 Transient Wave Packets

The capabilities of the new wave model to capture dispersion and wave propagation in increased water depth is validated for a focused wave packet Clauss and L. (1997). Nonlinear

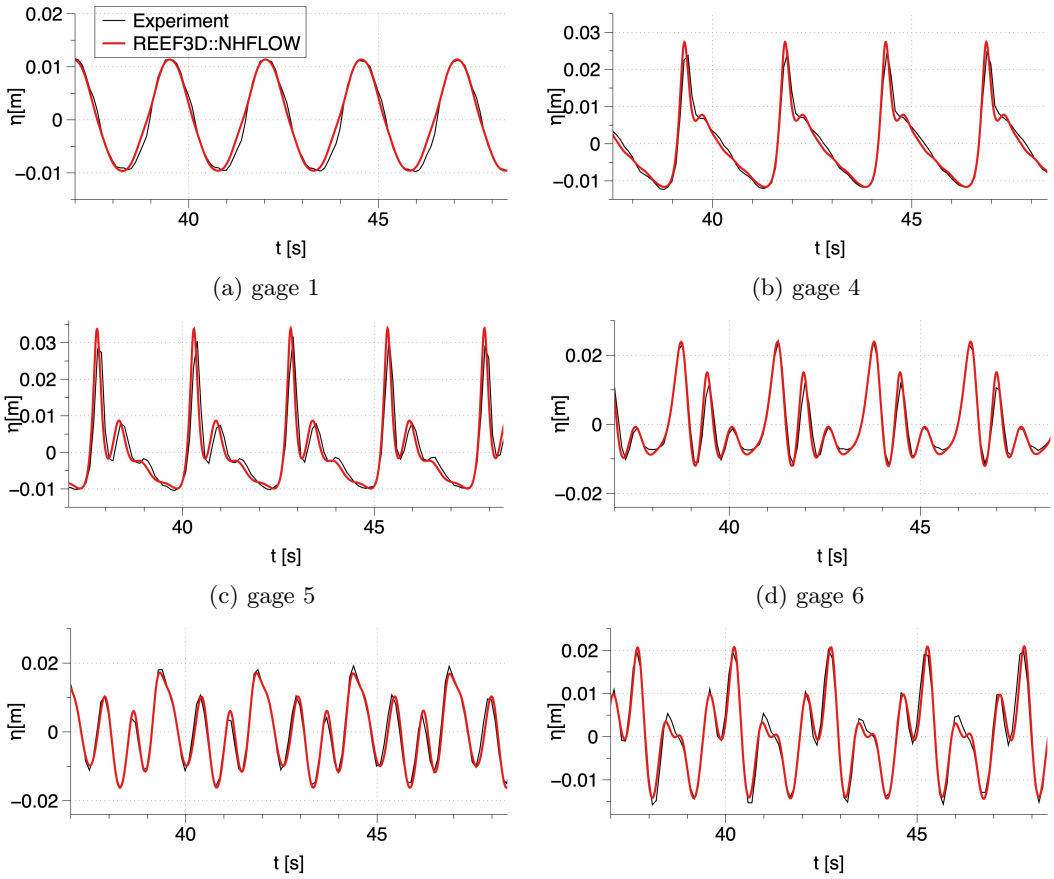

(a) gage 1

(b) gage 4

(c) gage 5

(d) gage 6

(e) gage 7

(f) gage 8

Figure 4: The surface elevations of the wave transformation over a submerged bar using REEF3D::NHFLOW with 1400 cells in x-direction and 3 non-uniform vertical layers.

transient wave packets use a synthetic Fourier spectrum L. et al. (2002). The spectrum is scaled to a desired amplitude distribution and a series of linear wave components is created. Their phase is controlled so that the components focus at the selected location and time. Using the Fourier spectrum instead of e.g. the JONSWAP spectrum has the advantage that steep focused waves can be created without previous breaking of individual wave components. The experiments for this case have been performed in the Large Wave Flume (GWK), Hannover, Germany Pakozdi (2005). The data set has been previously used as a validation case for the REEF3D's CFD model Bihs et al. (2019) and fully nonlinear potential flow model FNPF Bihs et al. (2020).

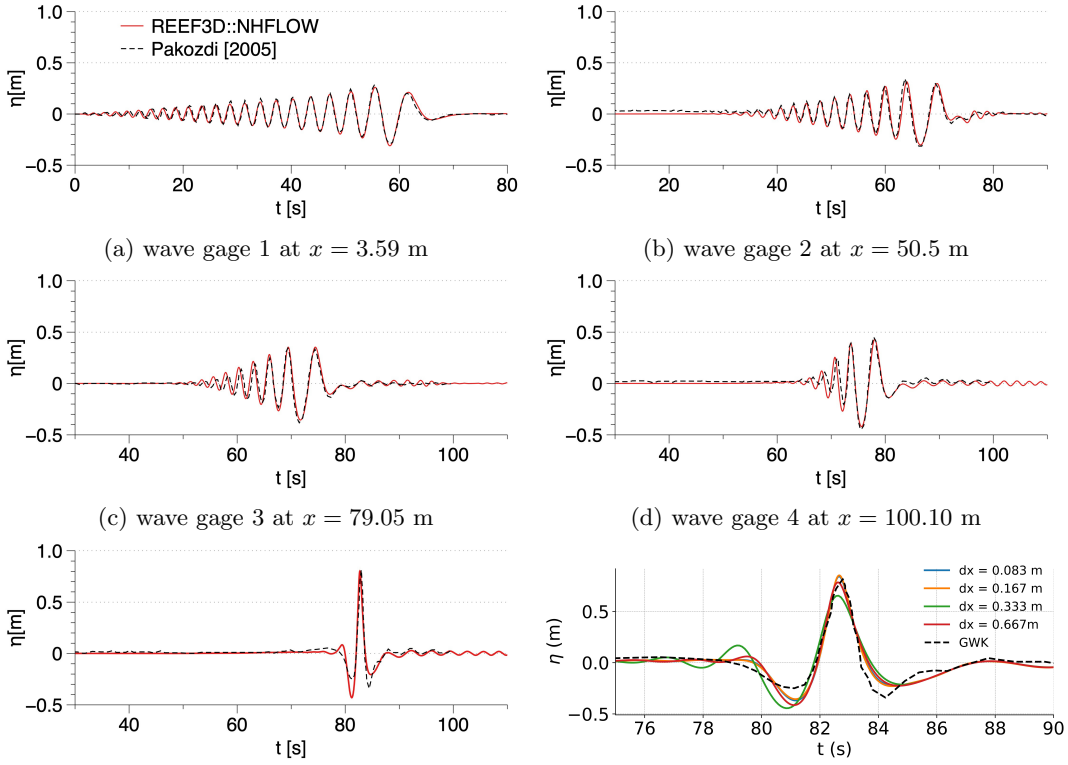

(a) wave gage 1 at $x = 3.59$ m

(b) wave gage 2 at $x = 50.5$ m

(c) wave gage 3 at $x = 79.05$ m

(d) wave gage 4 at $x = 100.10$ m

(e) wave gage at the focus point at $x = 126.21$ m

(f) grid convergence at the focus point

Figure 5: The comparison between the simulated time series and the experimental measurements at all wave gages in the numerical wave tank for the focusing wave packet. (e) the surface elevation at the focusing point. (f) grid convergence study at the focus point.

The Large Wave Flume is 300 m long and the still water depth is $d = 4.01$ m. The wave packets are generated by a piston-type wavemaker. The distance from the wavemaker to the focus point is $x_f = 126.21$ m and the focusing time is $t_f = 83$ s. Wave gages were placed $x = 3.59$ m, 50.5 m, 79.05 m, 100.10 m and 126.21 m away from the piston. The numerical model uses a two-dimensional numerical wave tank with a length of 250 m. The numerical mesh has 1500 horizontal elements, resulting in a $dx = 0.167$ m. Three vertical layers with exponential stretching (stretching factor $\alpha = 2.5$) towards the free surface were sufficient to capture the dispersive character of the wave components accurately.

The numerical results are compared against the experimental data at five different lo-

cations in Fig. 5, ranging from the vicinity of the wave generation ($x = 3.59$ m from the wavemaker) up to the focusing location ($x = 126.21$ m from the wavemaker). As can be seen, from wave gage WG 1, the method of transient wave packets at first creates wave components of smaller wavelength that travel relatively slower than the wave components with increased length that are generated successively. Due to the dispersive nature of the created waves, all wave crests then intersect at the pre-defined focus point. After the focusing point, the wave packets decompose again into multiple components. WGs 2-4 show the focusing process as the components are moving closer together and fewer and fewer wave crests are visible. The presented numerical model results compare well against the experimental data. Both the wave elevation at the focusing point as well as the phases of the components are predicted accurately during the focusing process.

3.4 Breaking waves on a mild slope

The model is used to simulate breaking waves over a mild slope following the configurations in Kimmoun and Branger (2007). The physical experiment was conducted in the EGIM/ECM wave tank in Marseilles, which is 17 m and 0.65 m wide. The water depth in front of the wavemaker is 0.705 m. A 1/15 slope is arranged at 4.2 m downstream from the wavemaker. The slope continues for 12.8 m and rises up to 0.8533. The numerical wave tank (NWT) follows the same configuration in a two-dimensional setup, neglecting the transverse direction. A 5^{th}-order Stokes wave is generated at the left-hand inlet with a one-wavelength relaxation zone. The incident wave has a wave height of 11.4 cm and a period of 1.275 s, which gives a wavelength of 2.41 m at the wave generation zone. The slope similarity number is 0.28, which corresponds to a spilling breaker Ting and Kirby (1995, 1996). The simulation time is the same as the experiment: 326.4 s, corresponding to 256 wave cycles.

The wave crest height H_c at breaking is used to study the horizontal grid convergence with 4 cell sizes 0.0125, 0.025, 0.5 and 1.0 m, as shown in Fig. 7. The prediction converges after a 0.025 m cell size. 5 vertical σ cells with a stretching factor of 2.5 towards the free surface are used in all cases. With $dx = 0.025$ m and $CFL = 0.5$, the simulation takes 629.9 s on a 12-core MacBook Pro with Apple M4 Max processors. The numerical wave tank configurations and the simulated free surface and horizontal velocities are visualised in Fig. 6. The accumulating spatial wave surface profile along the x-axis during the 129 to 256 wave periods time frame are plotted together to form an envelope, which is compared to the measured maximum wave crests and troughs in the experiment Kimmoun and Branger (2007), as shown in Fig. 9. The wave height at breaking point H_b in the simulation is 13.85 cm, which is close to the experiment at 14.0 cm, and the theoretical prediction of 13.9 cm following the formulation in Miche (1951). The wave profile envelop shows the correct representation of the shoaling process with increased wave crest and the correct wave breaking onset location as the maximum wave crest is reached at the same location as the measured data. The decrease in wave height after wave breaking in the simulation also aligns with the experimental observations, indicating a similar wave energy dissipation due to the breaking process. The simulated surface elevation towards the swash zone shows a discrepancy with the experiment at around 13.5 m, but stabilizes to a similar level as in the experiment passing $x =$ 14 m. Despite this discrepancy, the simulated wave breaking process is generally agreeable with the experiment.

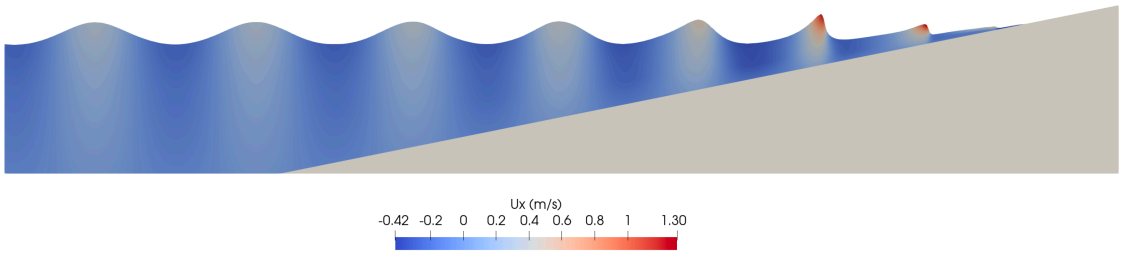

Figure 6: Free surface and horizontal velocity at a breaking wave event in the numerical simulation at $t = 10.6$ s.

[b]0.3

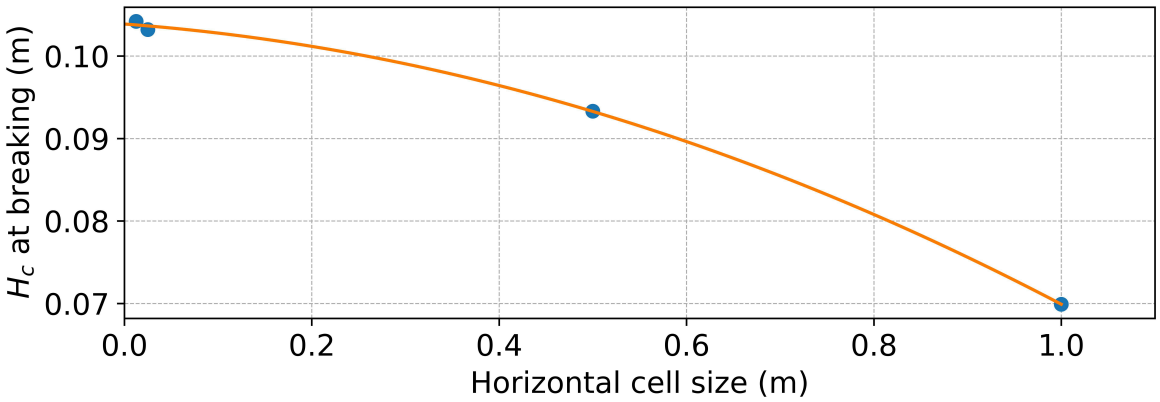

Figure 7: grid convergence in terms of wave crest height at breaking

[b]0.5

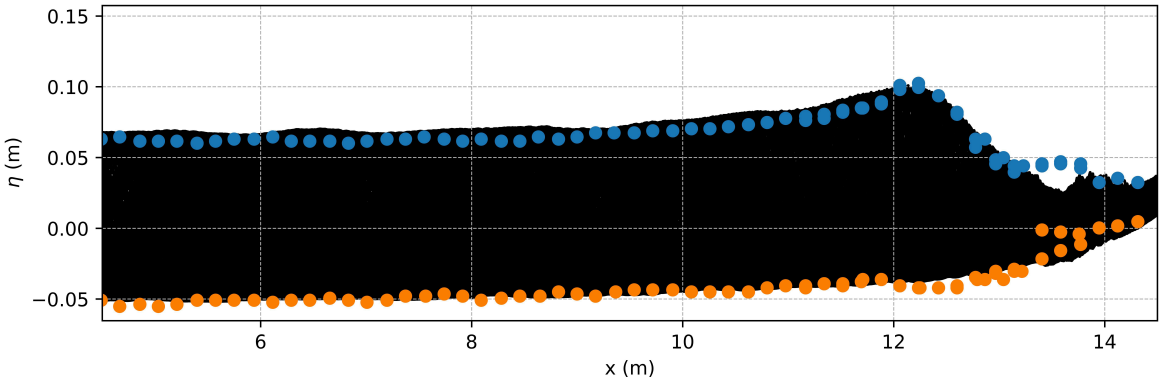

Figure 8: Wave profile envelop corresponding to 129 to 256 wave cycles

Figure 9: (a) grid convergence for breaking wave crest height with four different cells; (b) Simulated wave profile envelop corresponding to 129 to 256 wave cycles (black lines). The blue and orange dots are the maximum wave crest and trough in the experiment Kimmoun and Branger (2007).

4 Real-World Applications

4.1 Naissaar Harbor

Naissaar island is located northwest of Tallinn and the Naissaar harbor is found on the east coast of the island facing the Gulf of Finnland. The long-distance open sea in the Gulf of Finnland from St. Petersburg to Tallinn allows for a long fetch and the development of a strong wind wave system from the east. There is a shoal in the northeast direction outside the harbor with a water depth of only 3 to 5 m. From the shoal towards the harbor, the water depth increases first up to 30 m before it decreases again rapidly near the coastline. The wave transformations induced by the bathymetry outside the harbor and the effect of the existing breakwater are simulated with the proposed model.

A narrow-spreading wind sea is generated from the East boundary and numerical beaches are allocated at the north and south boundary to reduce unrealistic wave reflection from these side boundaries. The horizontal extend of the simulation domain is 4km $\times$ 3km with a mesh resolution of 1600 $\times$ 1200 $\times$ 5 cells, resulting in a total of 9.6 million cells. The calculations are run on UNINETT Sigma2's supercomputer Betzy using 512 cores. The simulated wave surface elevation in the entire domain is shown in Fig. 11. The water depth variation leads to an inhomogeneous wave field in the adjacent offshore area. Wave shoaling, refraction and diffraction can be observed as the waves propagate towards the coastline and the harbor. For the simulated wave condition, the breakwater shows the desired effect of reducing the wave height at the inner harbor. Spectral wave gages G1 and G2 in Fig. 12 show the magnitude of the incoming wave energy. Gages G3 and G4 are placed inside the harbor and reveal significantly lower waves, confirming the effectiveness of the breakwater layout. However, the offshore wave directionality might lead to different results for the breakwater's effectiveness.

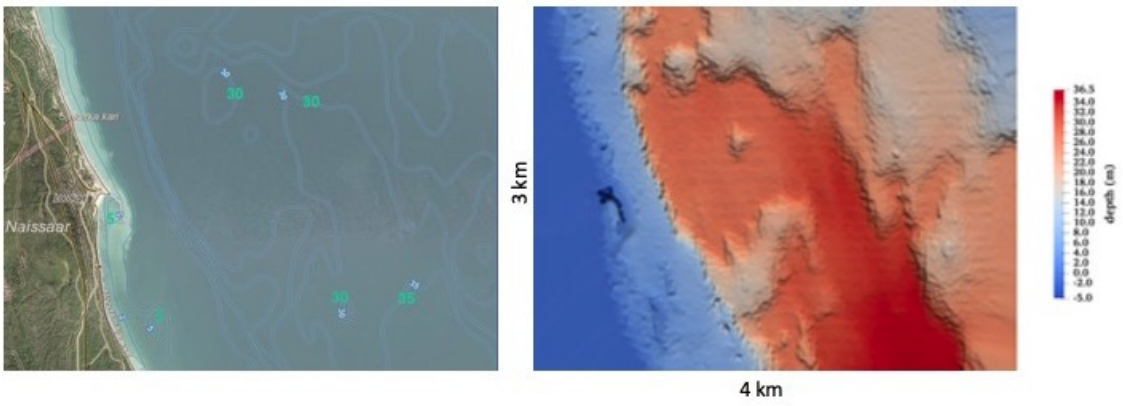

Figure 10: Satellite image and seafloor bathymetry of the coastal area around the Estonian harbor Naissaar.

4.2 Nazaré Surf Waves

Some of the world's most extreme coastal breaking waves can be found in Nazaré, Portugal (see Fig. 13). The challenging wave conditions are an attraction for professional surfers, giving

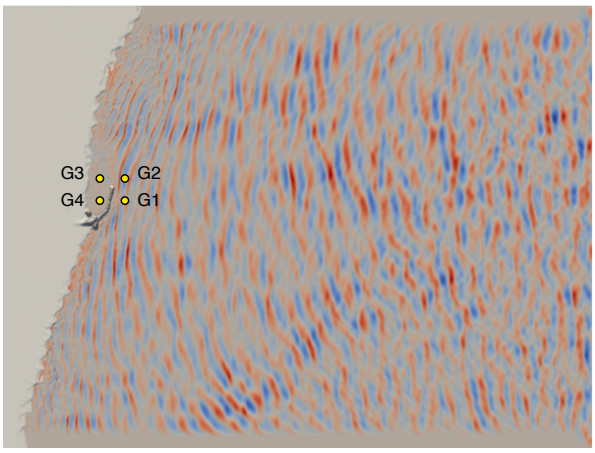

Figure 11: Free surfaces elevation with REEF3D::NHFLOW for the Estonian harbor Naissaar.

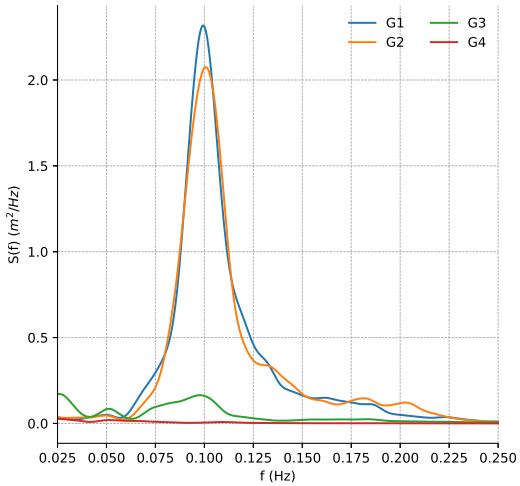

Figure 12: Wave spectra for the different locations around the breakwater at Naissaar harbor, Estonia.

the opportunity to surf some of the highest waves ever measured. As can be seen in Fig. 13b, a deep ocean trench meanders away from the coastal, giving seafloor a unique topography. The specific geometry of the Nazaré Canyon is responsible for the extreme breaking wave conditions, as high waves can propagate towards coast over the deep Canyon without breaking. At the same time, the overall coastal geography influences the waves transformation through refraction effects that bring waves from both North and South towards the front of the cliff at the lighthouse.

There, refraction forces the waves to travel at an angle over the side walls of the canyon, leading to intensive shoaling and consequently massive plunging breaking waves. As part of EEA Norway-Portugal project "Coastal wave modeling in the world surfing reserve Ericeira", surf wave conditions are modeled for delivering more reliable wave information to the surfing community in Ericeira. Naizaré is located ca. 80 km north of Eirceira and is an intriguing test case for the new wave model, as it includes unique and extreme sea floor changes.

Fig. 13b shows the seafloor bathymetry used within NHFLOW. The seafloor data is obtained from the EMODNet data base with a 115 m spacing between the data points and from a LiDAR scan of the near-coastal area with 1 5m resolution.The extend of the computational domain in x-direction is 16.8 km and in y-direction, it is 11 km. The horizontal mesh resolution is a uniform $dx = dy = 5$ m, resulting in a 3360×2200 mesh. With a vertical resolution of 8 non-uniformly spaced elements, the total cell count is ca. 59.1 million cells. The simulations are run on the supercomputer Betzy provided by UNINETT Sigma2, utilizing 512 cores. As input, irregular short crested waves with narrow directional spreading are used with significant wave height of $H_s = 8$ m and $T_p = 12$ s Fig. 13c shows the instantaneous free surface elevation for the simulation domain. The wave pattern over the northern side wall of the underwater canyon stands out: here the waves are significant higher due to the shoaling effects, which then results in the plunging surf waves the Nazaré location is known for. This test case highlights NHFLOW's capability as a coastal wave model that can handle waves propagating over strongly irregular bathymetry.

5 Conclusions

The new non-hydrostatic flow and wave model REEF3D::NHFLOW is presented in the current paper. Through the use of the σ-coordinate grid, a Godunov-type scheme with shock-capturing properties and WENO flux reconstruction, the model can predict wave transformation in an efficient and accurate manner. In addition, the model is fully parallelized based on the domain decomposition strategy and can thus be employed for large-scale wave propagation problems. The model is validated against several benchmark cases to assess its numerical performance. The fifth-order Stokes wave simulation demonstrates the model's ability to represent steep, dispersive waves. Accurate reproduction of wave transformation and dispersion is observed in the submerged bar test, with results aligning well with measurements. The model also captures the evolution of a focused wave packet in deep water, showing strong agreement with experimental data. In the breaking wave case over a sloping beach, the model reliably predicts wave height, breaking location, and energy dissipation. These validations collectively confirm the robustness and accuracy of the model. The wave modeling of the Estonian harbor Naissaar and the surf waves at Nazaré, Portugal gives an outlook for possible real-world applications of the presented numerical model. Though the model has shown

(a) Breaking wave at the Fort of São Miguel Arcanjo lighthouse Nazaré, Portugal (photo: Luis Ascenso, licensed under the terms of the cc-by-2.0)

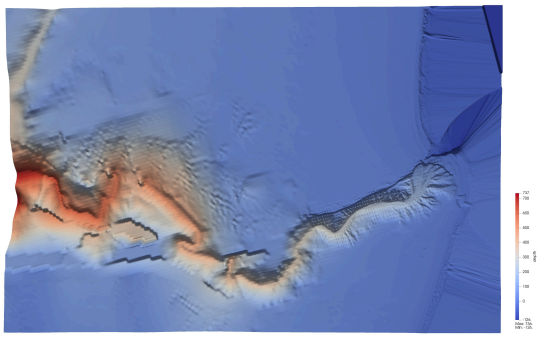

(b) Coastal bathymetry in front of the Nazaré lighthouse with the Nazaré Canyon.

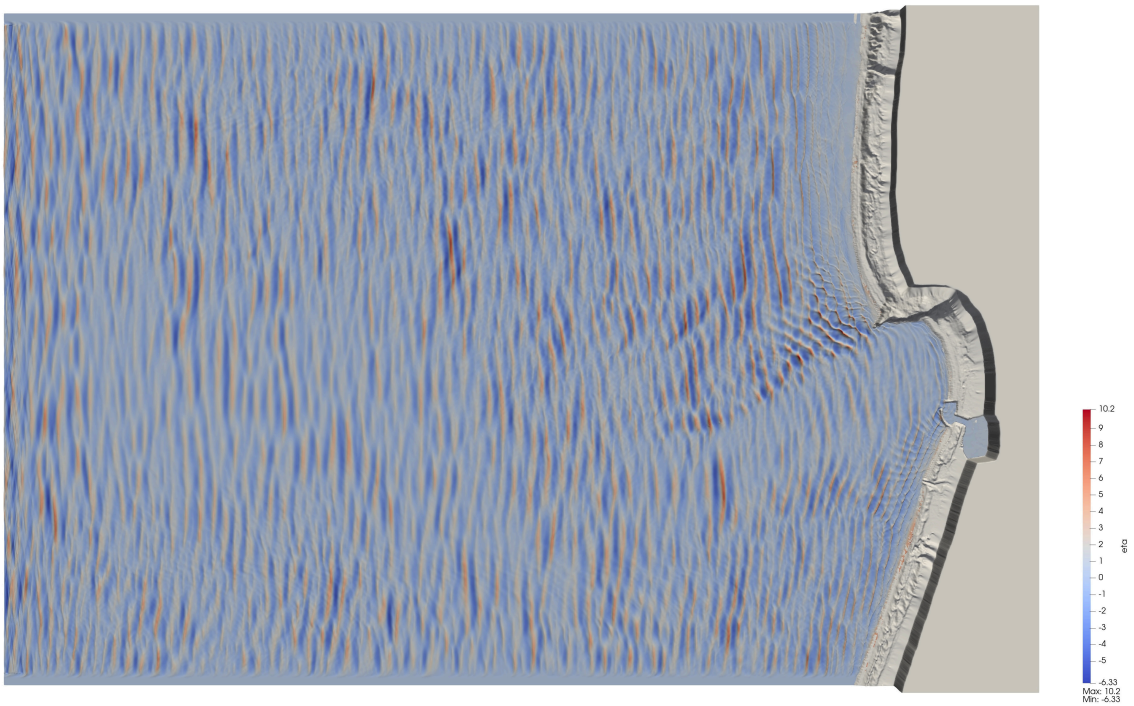

(c) Free surface pattern highlighting the intense shoaling and breaking wave conditions in front of the lighthouse cliff.

Figure 13: Nazaré, Portugal.

positive validations and promising application potentials, further developments are planned for increased engineering relevance. A dedicated wave-breaking model may be expected to provide a more accurate prediction for a wider range of breaker types. The nature of the model allows for multi-physics expansions. Thus, wind effect, current, sediment transport and wave-structure interaction will be incorporated in the future.

Acknowledgements

The authors thank the financial and technical support from the EEA Norway-Baltic project EMP480 - "Solutions to current and future problems on natural and constructed shorelines, eastern Baltic Sea". We are also grateful for the bathymetry data for Naissar provided by Rain Mannikus, Tallinn University of Technology. Thanks goes to Tiago Gomes from blueOASIS for the Nazaré bathymetry data, as part of the EEA Norway-Portugal project "Coastal wave modeling in the world surfing reserve Ericeira". The authors thank the funding by the European Union (ERC, PARTRES, 101045646). Views and opinions expressed are however those of the authors only and do not necessarily reflect those of the European Union or the European Research Council Executive Agency. Neither the European Union nor the granting authority can be held responsible for them. The simulations in section 4 were performed on the supercomputer Betzy provided by Sigma2 - the National Infrastructure for High-Performance Computing and Data Storage in Norway.

References

Aggarwal, A., Alagan Chella, M., Bihs, H. and Myrhaug, D. (2020). Properties of breaking irregular waves over slopes. *Ocean Engineering*, **216**, 108098. ISSN 0029-8018. /10.1115/1.4068917https://doi.org/10.1016/j.oceaneng.2020.108098.

Aggarwal, A., Bihs, H., Myrhaug, D. and Alagan Chella, M. (2019*a*). Characteristics of breaking irregular wave forces on a monopile. *Applied Ocean Research*, **90**(101846).

Aggarwal, A., Bihs, H. Shirinov, S. and Myrhaug, D. (2019*b*). Estimation of breaking wave properties and their interaction with a jacket structure. *Journal of Fluids and Structures*, **91**(102722).

Ahmad, N., Kamath, A. and Bihs, H. (2020). 3d numerical modelling of scour around a jacket structure with dynamic free surface capturing. *Ocean Engineering*, **200**, 107104. ISSN 0029-8018. /10.1115/1.4068917https://doi.org/10.1016/j.oceaneng.2020.107104.

Ashby, S.F. and Falgout, R.D. (1996). A parallel mulitgrid preconditioned conjugate gradient algorithm for groundwater flow simulations. *Nuclear Science and Engineering*, **124**(1), 145–159.

Beji, S. and Battjes, J.A. (1993). Experimental investigation of wave propagation over a bar. *Coastal Engineering*, **19**, 151–162.

Bihs, H., Kamath, A., Alagan Chella, M., Aggarwal, A. and Arntsen, Ø.A. (2016). A new level set numerical wave tank with improved density interpolation for complex wave hydrodynamics. *Computers & Fluids*, **140**, 191–208.

Bihs, H., Kamath, A., Alagan Chella, M. and Arntsen, Ø.A. (2019). Extreme wave generation, breaking, and impact simulations using wave packets in reef3d. *Journal of Offshore Mechanics and Arctic Engineering*, **141**(041802-1).

Bihs, H., Pakozdi, C. and Kamath, A. (2020). REEF3D::FNPF—a flexible fully nonlinear potential flow solver. *Journal of Offshore Mechanics and Arctic Engineering*, **142**(041902-1).

Casulli, V. and Zanolli, P. (2002). Semi-implicit numerical modeling of nonhydrostatic free-surface flows for environmental problems. *Mathematical and Computer Modelling*, **36**(9), 1131–1149. ISSN 0895-7177. /10.1115/1.4068917https://doi.org/10.1016/S0895-7177(02)00264-9.

Chen, Q., Kelly, D.M. and Zang, J. (2019). On the relaxation approach for wave absorption in numerical wave tanks. *Ocean Engineering*, **187**, 106210. ISSN 0029-8018. /10.1115/1.4068917https://doi.org/10.1016/j.oceaneng.2019.106210.

Chorin, A. (1968). Numerical solution of the Navier-Stokes equations. *Mathematics of Computation*, **22**, 745–762.

Clauss, G.F. and L., K.W. (1997). A new tool for seakeeping test - nonlinear transient wave packets. *8th International Conference on the Behaviour of Off-Shore Structures, Delft, The Netherlands*.

Dempwolff, L.C., Windt, C., Bihs, H., Melling, G., Holzwarth, I. and Goseberg, N. (2023). Hydrodynamic coupling of multi-fidelity solvers in reef3d with application to ship-induced wave modelling. *Coastal Engineering*, 104452. ISSN 0378-3839. /10.1115/1.4068917https://doi.org/10.1016/j.coastaleng.2023.104452.

Ducrozet, G., Bonnefoy, F., Le Touzé, D. and Ferrant, P. (2012). A modified high-order spectral method for wavemaker modeling in a numerical wave tank. *European Journal of Mechanics B/Fluids*, **34**, 19–34.

Engsig-Karup, A., Bingham, H. and Lindberg, O. (2009). An efficient flexible-order model for 3d nonlinear water waves. *Journal of Computational Physics*, **228**(6), 2100–2118. ISSN 0021-9991. /10.1115/1.4068917https://doi.org/10.1016/j.jcp.2008.11.028.

Fenton, J.D. (1985). A fifth order Stokes theory for steady waves. *Journal of Waterway, Port, Coastal and Ocean Engineering*, **111**(2), 216–234.

Forum, M.P. (1994). Mpi: A message-passing interface standard. Technical report, USA.

Gottlieb, S. and Shu, C.W. (1998). Total variation diminishing runge-kutta schemes. *Mathematics of Computation*, **67**(221), 73–85.

Grilli, S.T., Subramanya, R., Svendsen, I.A. and Veeramony, J. (1994). Shoaling of solitary waves on plane beaches. *Journal of Waterway, Port, Coastal, and Ocean Engineering*, **120**(6), 609–628.

Harten, A., Lax, P. and van Leer, B. (1983). On upstream differencing and godunov-type schemes for hyperbolic conservation laws. *SIAM Review*, **25**(1).

Higuera, P., Lara, L.J. and Losada, I.J. (2013). Realistic wave generation and active wave absorption for Navier-Stokes models application to OpenFOAM. *Coastal Engineering*, **71**, 102–118.

Jacobsen, N.G., Fuhrman, D.R. and Fredsøe, J. (2012). A wave generation toolbox for the open-source CFD library: OpenFOAM. *International Journal for Numerical Methods in Fluids*, **70**(9), 1073–1088.

Jiang, G.S. and Shu, C.W. (1996). Efficient implementation of weighted ENO schemes. *Journal of Computational Physics*, **126**, 202–228.

Kamath, A., Alagan Chella, M., Bihs, H. and Arntsen, Ø.A. (2017). Energy transfer due to shoaling and decomposition of breaking and non-breaking waves over a submerged bar. *Engineering Applications of Computational Fluid Mechanics*, **11**(1), 450—466.

Keerthi Raaj, S., Vijay, K.G., Neelamani, S., Saha, N. and Sundaravadivelu, R. (2023). Gravity wave interaction with a composite pile–rock breakwater. *Journal of Offshore Mechanics and Arctic Engineering*, **146**(3), 031903. ISSN 0892-7219. /10.1115/1.406891710.1115/1.4064013.

Kimmoun, O. and Branger, H. (2007). A particle image velocimetry investigation on laboratory surf-zone breaking waves over a sloping beach. *Journal of Fluid Mechanics*, **588**, 353–397. /10.1115/1.406891710.1017/S0022112007007641.

Kinnas, S. (2007). Notes on fifth-order gravity wave theory. Technical report, Offshore Technology Research Center, UT Austin.

Kumaran, V., Venkateswarlu, V., Raja Pandi, R. and Nishad, C.S. (2024). Hydrodynamic performance of an inverted trapezoidal breakwater with permeable retrofit. *Journal of Offshore Mechanics and Arctic Engineering*, **147**(1), 011206. /10.1115/1.406891710.1115/1.4065772.

L., K.W., Clauss, G.F. and Henning, J. (2002). Tailor made freak waves within irregular seas. *21st International Conference on Offshore Mechanics and Arctic Engineering, Oslo, Norway*, **4**, 759–768.

Li, B. (2008). A 3-d model based on navier–stokes equations for regular and irregular water wave propagation. *Ocean Engineering*, **35**(17), 1842–1853. ISSN 0029-8018. /10.1115/1.4068917https://doi.org/10.1016/j.oceaneng.2008.09.006.

Li, B. and Fleming, C. (2001). Three-dimensional model of navier-stokes equations for water waves. *Journal of Waterway Port Coastal and Ocean Engineering*, **127**. /10.1115/1.406891710.1061/(ASCE)0733-950X(2001)127:1(16).

Li, B. and Fleming, C.A. (1997). A three dimensional multigrid model for fully nonlinear water waves. *Coastal Engineering*, **30**(3–4), 235–258.

Liang, Q. and Marche, F. (2009). Numerical resolution of well-balanced shallow water equations with complex source terms. *Advances in Water Resources*, **32**, 873–884.

Lin, P. and Li, C.W. (2002). A σ-coordinate three-dimensional numerical model for surface wave propagation. *International Journal for Numerical Methods in Fluids*, **38**(11), 1045–1068. /10.1115/1.4068917https://doi.org/10.1002/fld.258.

Ma, G., Kirby, J.T. and Shi, F. (2013). Numerical simulation of tsunami waves generated by deformable submarine landslides. *Ocean Modelling*, **69**, 146–165. ISSN 1463-5003. /10.1115/1.4068917https://doi.org/10.1016/j.ocemod.2013.07.001.

Ma, G., Shi, F. and Kirby, J.T. (2012). Shock-capturing non-hydrostatic model for fully dispersive surface wave processes. *Ocean Modeling*, **43–43**, 22–35.

Madsen, R. (2009). *Udvikling af en skalerbar parallel løser af Laplaceligningen for ikke-lineære vandbølger*. Master's thesis, Danmarks Tekniske Universitet, DTU Informatik.

Martin, T. and Bihs, H. (2021). A non-linear implicit approach for modelling the dynamics of porous tensile structures interacting with fluids. *Journal of Fluids and Structures*, **100**, 103168. ISSN 0889-9746. /10.1115/1.4068917https://doi.org/10.1016/j.jfluidstructs.2020.103168.

Martin, T., Kamath, A. and Bihs, H. (2021). Accurate modeling of the interaction of constrained floating structures and complex free surfaces using a new quasistatic mooring model. *International Journal for Numerical Methods in Fluids*, **93**(2), 504–526. /10.1115/1.4068917https://doi.org/10.1002/fld.4894.

Miche, R. (1951). Le pouvoir réfléchissant des ouvrages maritimes exposés à l'action de la houle. *Ann. Ponts Chaussées*, **121**, 285–319.

Pakozdi, C. (2005). Numerische Simulation nichtlinearer transienter Wellengruppen. Report, Technical University Berlin.

Pakozdi, C., Bihs, H. and Kamath, A. (2021). Reef3d wave generation interface for commercial computational fluid dynamics codes. *Journal of Offshore Mechanics and Arctic Engineering*, **143**(031902-1).

Pákozdi, C., Wang, W., Kamath, A. and Bihs, H. (2021). Reduction of the wave propagation error of a sigma grid based numerical tank using a vertical spacing based on the constant truncation error. *Ocean Engineering*, **239**, 109741. ISSN 0029-8018. /10.1115/1.4068917https://doi.org/10.1016/j.oceaneng.2021.109741.

Peric, M. and Ferziger, J. (2001). *Computational Methods for Fluid Dynamics*. Springer.

Praveen, K.M., Venkateswarlu, V. and and, D.K. (2022). Wave transformation due to finite floating elastic plate with abrupt change in bottom topography. *Ships and Offshore Structures*, **17**(8), 1824–1842. /10.1115/1.406891710.1080/17445302.2021.1946308.

Reidulff, K., Wang, W., Kamath, A. and Bihs, H. (2023). Wave environment analysis at norwegian harbours for land-based aquaculture facilities using a combined phase-averaging and phase-resolving numerical modelling approach. *Journal of Coastal and Hydraulic Structures*, **3**. /10.1115/1.406891710.59490/jchs.2023.0031.

Roeber, V., Cheung, K. and Kobayashi, M. (2010). Shock-capturing boussinesqtype model for nearshore wave processes. *Coastal Engineering*, **57**, 407–423.

Roeber, V. and Cheung, K.F. (2012). Boussinesq-type model for energetic breaking waves in fringing reef environments. *Coastal Engineering*, **70**, 1–20. ISSN 0378-3839. /10.1115/1.4068917https://doi.org/10.1016/j.coastaleng.2012.06.001.

Sasikumar, A., Kamath, A. and Bihs, H. (2020). Modelling porous coastal structures using a level set method based vrans-solver on staggered grids. *Coastal Engineering Journal*, **62**(2), 198–216.

Stelling, G. and Zijlema, M. (2003). An accurate and efficient finite-difference algorithm for non-hydrostatic free-surface fow with application to wave propagation. *International Journal for Numerical Methods in Fluids*, **43**, 1–23.

Ting, F.C.K. and Kirby, J.T. (1995). Dynamics of surf-zone turbulence in a strong plunging breaker. *Coastal Engineering*, **24**, 177–204.

Ting, F.C.K. and Kirby, J.T. (1996). Dynamics of surf-zone turbulence in a spilling breaker. *Coastal Engineering*, **27**, 131–160.

van der Vorst, H. (1992). BiCGStab: A fast and smoothly converging variant of Bi-CG for the solution of nonsymmetric linear systems. *SIAM Journal on Scientific and Statistical Computing*, **13**, 631–644.

Wang, G., Martin, T., Huang, L. and Bihs, H. (2022*a*). Numerical investigation of the hydrodynamics of a submersible steel-frame offshore fish farm in regular waves using cfd. *Ocean Engineering*, **256**, 111528. ISSN 0029-8018. /10.1115/1.4068917https://doi.org/10.1016/j.oceaneng.2022.111528.

Wang, W., Pákozdi, C., Kamath, A. and Bihs, H. (2023). Fully nonlinear phase-resolved wave modelling in the norwegian fjords for floating bridges along the e39 coastal highway. *Journal of Ocean Engineering and Marine Energy*, **9**(3), 567–586. /10.1115/1.406891710.1007/s40722-023-00284-z.

Wang, W., Pákozdi, C., Kamath, A., Martin, T. and Bihs, H. (2022*b*). Hydrodynamic coupling of viscous and non-viscous numerical wave solutions within the open-source hydrodynamics framework REEF3D. *Journal of Offshore Mechanics and Arctic Engineering*, **144**(4). ISSN 0892-7219. /10.1115/1.406891710.1115/1.4053848. 041903.

Wang, W.W., Kamath, A., Pakozdi, C. and Bihs, H. (2020*a*). A comparison of different wave modelling techniques in an open-source hydrodynamic framework. *Journal of Marine Science and Engineering*, **8**(7), 526.

Wang, W.W., Martin, T., Kamath, A. and Bihs, H. (2020*b*). An improved depth-averaged nonhydrostatic shallow water model with quadratic pressure approximation. *International Journal for Numerical Methods in Fluids*, **92**(8), 803–824.

Wang, W.W., Pakozdi, C., Kamath, A. and Bihs, H. (2022*c*). A flexible fully nonlinear potential flow model for wave propagation over the complex topography of the norwegian coast. *Applied Ocean Research*, **122**(103103).

Zijlema, M., Stelling, G. and Smit, P. (2005). Further experiences with computing non-hydrostatic free-surface flows involving water waves. *International Journal for Numerical Methods in Fluids*, **48**, 169–197.